



## Article

# A Pathway for Aldol Additions Catalyzed by L-Hydroxyproline-Peptides via a $\beta$ -Hydroxyketone Hemiaminal Intermediate

 Lo'ay Ahmed Al-Momani <sup>1,\*</sup> , Heinrich Lang <sup>2</sup> and Steffen Lüdeke <sup>3,4,\*</sup> 
<sup>1</sup> Department of Chemistry, Faculty of Science, The Hashemite University, Zarqa 13133, Jordan

<sup>2</sup> Research Center for Materials, Architectures and Integration of Nanomembranes (MAIN), Research Group Organometallic Chemistry, Technische Universität Chemnitz, Rosenbergstraße 6, 09126 Chemnitz, Germany

<sup>3</sup> Institute of Pharmaceutical Sciences, Albert-Ludwigs-Universität Freiburg, Albertstraße 25, 79104 Freiburg, Germany

<sup>4</sup> Institute of Pharmaceutical and Biomedical Sciences (IPBS), Johannes Gutenberg-Universität Mainz, Staudingerweg 5, 55128 Mainz, Germany

\* Correspondence: loay.al-momani@hu.edu.jo (L.A.M.); sluedeke@uni-mainz.de (S.L.)

**Abstract:** While the use of L-proline-derived peptides has been proven similarly successful with respect to enantioselectivity, the physico-chemical and conformational properties of these organocatalysts are not fully compatible with transition state and intermediate structures previously suggested for L-proline catalysis. L-Proline or L-4-hydroxyproline catalysis is assumed to involve proton transfers mediated by the carboxylic acid group, whereas a similar mechanism is unlikely for peptides, which lack a proton donor. Herein, we prepared an array of hydroxyproline-based dipeptides through amide coupling of Boc-protected *cis*- or *trans*-4-L-hydroxyproline (*cis*- or *trans*-4-Hyp) to benzylated glycine (Gly-OBn) and L-valine (L-Val-OBn) and used these dipeptides as catalysts for a model aldol reaction. Despite the lack of a proton donor in the catalytic site, we observed good stereoselectivities for the *R*-configured aldol product both with dipeptides formed from *cis*- or *trans*-4-Hyp at moderate conversions after 24 h. To explain this conundrum, we modeled reaction cycles for aldol additions in the presence of *cis*-4-Hyp, *trans*-4-Hyp, and *cis*- and *trans*-configured 4-Hyp-peptides as catalysts by calculation of free energies of conformers of intermediates and transition states at the density functional theory level (B3LYP/6-31G(d), DMSO PCM as solvent model). While a catalytic cycle as previously suggested with L-proline is also plausible for *cis*- or *trans*-4-Hyp, with the peptides, the energy barrier of the first reaction step would be too high to allow conversions at room temperature. Calculations on modeled transition states suggest an alternative pathway that would explain the experimental results: here, the catalytic cycle is entered by the acetone self-adduct 4-hydroxy-4-methylpentan-2-one, which forms spontaneously to a small extent in the presence of a base, leading to considerably reduced calculated free energy levels of transition states of reaction steps that are considered rate-determining.

**Keywords:** proline catalysis; stereoselective synthesis; catalytic cycle; quantum chemical calculations



**Citation:** Al-Momani, L.A.; Lang, H.; Lüdeke, S. A Pathway for Aldol Additions Catalyzed by L-Hydroxyproline-Peptides via a  $\beta$ -Hydroxyketone Hemiaminal Intermediate. *Chemistry* **2023**, *5*, 1203–1219. <https://doi.org/10.3390/chemistry5020081>

Academic Editor: Angelo Frongia

Received: 2 April 2023

Revised: 2 May 2023

Accepted: 8 May 2023

Published: 10 May 2023

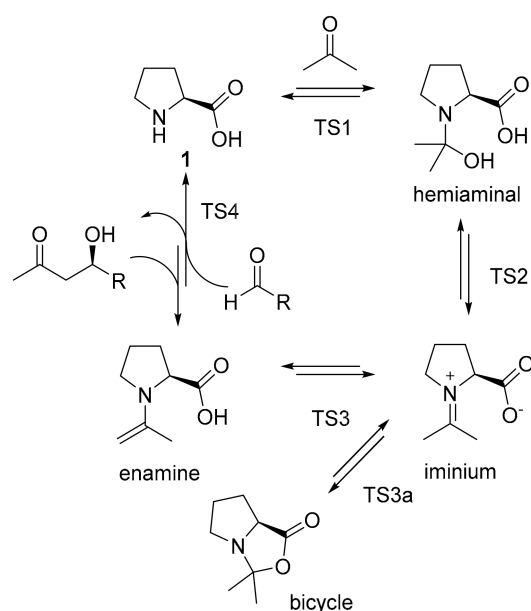


**Copyright:** © 2023 by the authors. Licensee MDPI, Basel, Switzerland. This article is an open access article distributed under the terms and conditions of the Creative Commons Attribution (CC BY) license (<https://creativecommons.org/licenses/by/4.0/>).

## 1. Introduction

Similar to the catalytic site of an enzyme, the geometric arrangement of nitrogen and oxygen atoms in the amino acid L-Proline (**1**) has the potential to catalyze asymmetric reactions—a discovery that led to a concept awarded with the Nobel Prize in Chemistry in 2021. In the last forty years, **1** has been used as a catalyst, for example, in the asymmetric Robinson annulation [1,2], the aldol condensation [3,4], and in the stereoselective Mannich reaction [5,6]. **1** also catalyzes an unconventional reaction via aldol condensation of  $\alpha$ -hydroxyketones and aldehydes to give  $\alpha,\beta$ -dihydroxyketones [7,8]. Several aspects have been discussed, such as the small size of **1**, its rigidity, inexpensiveness, and ready availability [9].

The reaction path of aldol reactions catalyzed by **1** had previously been under debate with respect to the intermediates and transition states determining the overall reaction rates and the stereoselectivity, respectively. The Houk–List pathway suggests an enamine intermediate being formed from **1** and the carbonyl substrate (Scheme 1) [10,11]. In stereoselective C,C-bond formation, proline's carboxylic acid group helps positioning a second carbonyl substrate in close proximity to the enamine moiety. While this is the rate-limiting step of aldol reactions catalyzed by **1** [12], the enamine, which serves as the activated electron donor, is of particular importance in the understanding of catalysis by **1** and derivatives thereof. Its formation involves different intermediates and transition states including the formation of a hemiaminal after addition of the first carbonyl substrate and the tautomerization of a zwitterionic iminium intermediate to the desired enamine. The latter transition competes with the formation of a bicyclic intermediate [13]. A direct involvement of this intermediate in stereoselective C–C-coupling has been proposed [14], but would be incompatible with observed enantio- and diastereoselectivities; therefore, a bicyclic intermediate is considered a merely parasitic by-product that competes with enamine formation [15].



**Scheme 1.** Catalytic cycle of L-proline-catalyzed aldol reaction of an aldehyde and acetone with intermediates and transition states (TS1 to TS4). TS3a is the transition state for the formation of a bicyclic parasitic by-product from the iminium intermediate.

Drawbacks of L-proline catalysis are its only moderate stereoselectivity and the necessity for comparably large amounts of catalyst, as the catalytic activity is low. The use of N-terminal L-proline peptides as organocatalysts seems a promising alternative [16,17]. It has been shown that some N-terminal L-proline tripeptides considerably increased activity and stereoselectivity compared to catalysis by **1**; however, both activity and stereoselectivity strongly depended on the choice of the L- or D-amino acid residue in addition to L-proline [18]. Effects on catalytic activity were explained by an optimal relative disposition of the secondary amine in the terminal L-proline and the carboxylic acid group of an L- or D-aspartic acid amide in position three. The stereoselectivity depends on the conformation of the tripeptide [18]; in the case of peptides of the Pro-Pro-Xaa-NH<sub>2</sub>-type, stereoselectivity clearly correlates with the *trans/cis* ratio of the Pro-Pro amide bond [19]. The notion of optimal distance and stereochemical arrangement in tripeptides is supported by the finding that neither activity nor stereoselectivity can be improved in tetrapeptides [20]. In the case of dipeptide catalysts, the reaction path of an aldol reaction may be more similar to the Houk–List pathway suggested for L-proline catalysis. The presence of a carboxylic

acid group seems to be beneficial for catalytic activity as the conversion in reactions catalyzed by Pro-NH<sub>2</sub> or Pro-Xaa-NH<sub>2</sub>, where Xaa can be any amino acid, is considerably lower [11,21,22]. Nevertheless, it could be shown that non-acidic N-terminal L-proline di-, tri-, tetra-, penta-, and hexapeptides whose C-terminal carboxylic acid group was masked as a methyl ester were still able to catalyze aldol reactions with moderate to high yield and moderate to high enantioselectivities [23,24].

Another important aspect is the increased conformational flexibility of peptide catalysts in comparison to **1** which might either stabilize or destabilize the geometry of a transition state or an intermediate throughout the catalytic cycle. However, if a defined chiral environment is still provided, it might even enhance selectivity [25,26]. Last but not least, both the chiral environment in the stereoselectivity-determining transition state and the rate-determining transition state are affected by the puckering of the proline ring. Proline adopts basically two preferred puckerings, C<sub>γ</sub>-*exo* and C<sub>γ</sub>-*endo* [27–30], which also applies to catalytic peptides with an N-terminal proline residue [26].

In *cis*-4-hydroxyproline (*cis*-4-Hyp, *cis*-**2**, Figure 1), C<sub>γ</sub>-*endo* is the most preferred puckering that would also allow the formation of an intramolecular hydrogen bond between the *cis*-4-hydroxy group and the carboxylic acid group. Similarly, **1** has a slight preference for C<sub>γ</sub>-*endo*. In contrast, in *trans*-4-hydroxyproline (*trans*-4-Hyp, *trans*-**2**, Figure 1), the 4-hydroxy group imposes a C<sub>γ</sub>-*exo* pucker. This is in accordance with the gauche empirical rule, an effect that also contributes to the outstanding stability of the collagen triple helix [31,32]. Intuitively, the ring puckering should also affect the stereoselectivity of reactions catalyzed by hydroxyprolines and related peptides. Surprisingly, in different reactions tested, the stereochemical outcome of reactions (aldol, Mannich and Michael asymmetric reactions) catalyzed by *cis*-**2** or *trans*-**2** was similar to **1** catalysis or even lower [33]. These observations prompted us to study the reaction channels leading to either an *R*- or an *S*-configured product in Hyp-catalysis or catalysis by Hyp-derived dipeptides in further detail, in particular, with respect to the role of the conformer distribution in organocatalysts, transition states, and intermediates.

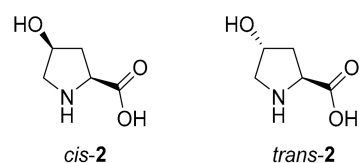
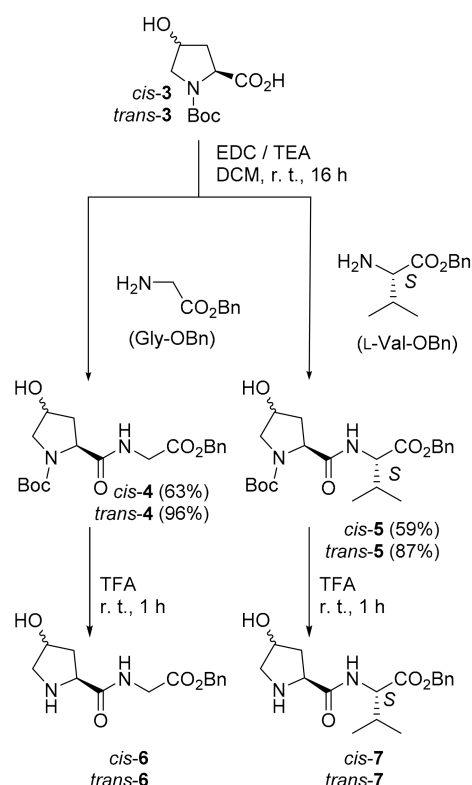


**Figure 1.** The two diastereomers of L-4-hydroxyproline (**2**).

We synthesized four Hyp-derived C-terminally protected dipeptides (*cis*-**6**, *trans*-**6**, *cis*-**7**, *trans*-**7**, Scheme 2) and performed the aldol addition of acetone to *p*-nitrobenzaldehyde (**8**) catalyzed by **6** or **7** as model reactions. To investigate whether catalysis of aldol additions with Hyp and Hyp-derived peptides follow a similar path as previously suggested for L-proline, we calculated the free energy differences of transition states and intermediates in Hyp and Hyp-dipeptide catalysis at the density functional theory level.



**Scheme 2.** Synthesis of dipeptide catalysts. A protection of the hydroxy groups of *cis*-3 or *trans*-3 was not necessary. Removal of the Boc group from dipeptides in the presence of anisole as a scavenger in dichloromethane was achieved in quantitative yields.

## 2. Materials and Methods

### 2.1. General Experimental Conditions

All reagents were of analytical grade. Solvents were dried by standard methods if necessary. TLC was carried out on aluminum sheets pre-coated with silica gel 60 F<sub>254</sub> (Merck, Darmstadt, Germany). Detection was accomplished by UV light ( $\lambda = 254$  nm). Preparative column chromatography was carried out on silica gel 60 (Merck, 40–63  $\mu$ m). <sup>1</sup>H NMR (500.3 MHz) spectra were recorded with a Avance III 500 spectrometer (Bruker, Ettlingen, Germany). CDCl<sub>3</sub> ( $\delta = 7.26$  ppm), H<sub>2</sub>O ( $\delta = 4.81$  ppm), and DMSO ( $\delta = 2.50$  ppm) were used as internal standards. <sup>13</sup>C{<sup>1</sup>H} NMR (125.8 MHz) spectra were calibrated with CDCl<sub>3</sub> ( $\delta = 77.00$  ppm) and DMSO-d<sub>6</sub> ( $\delta = 39.43$  ppm) as internal standard. IR spectra were recorded with a Nicolet IR200 FTIR-spectrometer (Thermo Fisher Scientific, Waltham, MA, USA). HR-MS spectra were measured with a micrOTOF QII mass spectrometer (Bruker Daltonics, Bremen, Germany). The enantiomeric excess (ee) values of the aldol reaction products were determined by chiral phase HPLC on an HP 1100 chromatography system (Agilent Technologies, Santa Clara, CA, USA) equipped with a Chiralpak AS-H column (Daicel, Osaka, Japan) using an *n*-hexane/isopropanol mixture (70:30) as eluent (UV 254 nm, flow rate 0.7 mL min<sup>−1</sup>, 25 °C).

### 2.2. Dipeptide Coupling

To a solution of 1.0 eq. of enantiomerically pure amino acid *cis*-3 or *trans*-3 (200 mg, 0.87 mmol) in dichloromethane (10 mL), 1.15 eq. of HOBt (50 mg, 1.0 mmol) were added, and the reaction mixture was cooled to 0 °C, followed by addition of 1.15 eq. of the *N*-terminally unprotected amino acids Gly-OBn (202 mg, 1.0 mmol) or L-Val-OBn (243 mg, 1.0 mmol). Afterwards, 3.0 eq. (263 mg, 2.61 mmol, 361 mL) of triethylamine (TEA) were added in a single portion and the reaction solution was allowed to stir for 10 min. at 0 °C. Then, 1.15 eq. (192 mg, 1.0 mmol) of 1-ethyl-3-(3-dimethylaminopropyl)carbodiimide (EDC) in dichloromethane (15 mL) were dropped gradually to the solution at 0 °C and stirred

at room temperature overnight. The reaction mixture was extracted with 1 M HCl, sat.  $\text{NaHCO}_3$  and finally with sat. NaCl. The collected dichloromethane layer was dried over anhyd.  $\text{Na}_2\text{SO}_4$ . The crude product was purified using column chromatography ( $\text{SiO}_2$ ). All products **4** and **5** were characterized by FT-IR and  $^1\text{H}$ ,  $^{13}\text{C}\{^1\text{H}\}$  NMR spectroscopy, and ESI-TOF mass-spectrometry (Figures S2–S17).

Dipeptides *cis*-**4** and *trans*-**4** were isolated as colorless viscous oils in a yield of 207 mg (63%) or 315 mg (96%).

*cis*-**4**:  $^1\text{H}$  NMR ( $\text{CDCl}_3$ )  $\delta$  = 7.62 (bs, 1H), 7.36–7.18 (m, 5H), 7.05 (bs, 1H), 5.08 (s, 2H), 4.85 (d,  $J$  = 8.5, 1H), 4.46–4.11 (m, 2H), 4.08–3.81 (m, 2H), 3.64–3.23 (m, 2H), 2.35–2.00 (m, 2H), 1.36 (s, 9H).  $^{13}\text{C}$  NMR ( $\text{CDCl}_3$ , several rotamers)  $\delta$  174.09, 171.13, 169.52, 169.18, 155.45, 154.22, 135.20, 128.61, 128.47, 128.33, 80.72, 70.78, 69.81, 67.12, 60.36, 59.99, 59.34, 56.83, 56.00, 41.62, 38.62, 36.39, 28.33, 21.01, 14.18. IR (neat,  $\text{cm}^{-1}$ ): 3307 (OH), 1742, 1667 (CO), 1189, 1131 (C–O). MS ( $\text{C}_{19}\text{H}_{26}\text{N}_2\text{O}_6$ ): calcd. 379.1869 ( $[\text{M}+\text{H}]^+$ ), exp. 379.1843 ( $[\text{M}+\text{H}]^+$ ).

*trans*-**4**:  $^1\text{H}$  NMR ( $\text{CDCl}_3$ )  $\delta$  = 7.40 (bs, 1H), 7.29–7.19 (m, 5H), 6.86 (bs, 1H), 5.06 (s, 2H), 4.32 (bs, 2H), 4.08–3.84 (m, 2H), 3.82–3.25 (m, 3H), 2.36–1.90 (m, 2H), 1.33 (s, 9H).  $^{13}\text{C}$  NMR ( $\text{CDCl}_3$ , several rotamers)  $\delta$  = 172.34, 171.64, 170.29, 168.54, 154.78, 153.86, 134.21, 127.60, 127.48, 127.32, 79.79, 68.61, 68.15, 66.09, 59.43, 58.76, 57.68, 53.97, 40.18, 38.49, 36.47, 27.29, 20.02, 13.17. IR (neat,  $\text{cm}^{-1}$ ): 3303 (OH), 1748, 1667 (C=O), 1159, 1127 (C–O). MS ( $\text{C}_{19}\text{H}_{26}\text{N}_2\text{O}_6$ ): calcd. 379.1869 ( $[\text{M}+\text{H}]^+$ ), exp. 379.1865 ( $[\text{M}+\text{H}]^+$ ).

Dipeptides *cis*-**5** and *trans*-**5** were isolated as colorless viscous oils in a yield of 213 mg (59%) or 320 mg (87%).

*cis*-**5**:  $^1\text{H}$  NMR ( $\text{CDCl}_3$ )  $\delta$  = 7.46 (d,  $J$  = 8.4, 1H), 7.32–7.20 (m, 5H), 6.77 (bs, 1H), 5.19–4.97 (m, 3H), 4.53–4.43 (m, 1H), 4.39 (d,  $J$  = 8.8, 1H), 4.25 (t,  $J$  = 20.2, 1H), 3.59–3.28 (m, 2H), 2.31–1.97 (m, 3H), 1.38 (s, 9H), 0.82 (m, 6H).  $^{13}\text{C}$  NMR ( $\text{CDCl}_3$ , several rotamers)  $\delta$  172.18, 170.16, 154.52, 134.39, 127.56, 127.39, 127.33, 79.57, 69.72, 68.80, 65.93, 59.18, 58.52, 56.69, 56.40, 55.99, 34.54, 30.20, 27.32, 17.88, 16.30. IR (neat,  $\text{cm}^{-1}$ ): 3283 (OH), 1737, 1701, 1664 (C=O), 1155, 1112 (C–O). MS ( $\text{C}_{22}\text{H}_{32}\text{N}_2\text{O}_6$ ): calcd. 421.2339 ( $[\text{M}+\text{H}]^+$ ), exp. 421.2338 ( $[\text{M}+\text{H}]^+$ ).

*trans*-**5**:  $^1\text{H}$  NMR ( $\text{CDCl}_3$ )  $\delta$  = 7.47 (bs, 1H), 7.33–7.11 (m, 5H), 6.63 (bs, 1H), 5.07 (q,  $J$  = 12.2, 2H), 4.55–4.20 (m, 3H), 3.92–3.15 (m, 3H), 2.45–1.77 (m, 3H), 1.35 (s, 9H), 0.81 (d,  $J$  = 6.8, 3H), 0.78 (d,  $J$  = 6.9, 3H).  $^{13}\text{C}$  NMR ( $\text{CDCl}_3$ , several rotamers)  $\delta$  = 171.98, 170.95, 170.50, 154.92, 153.93, 134.68, 134.43, 127.55, 127.34, 79.62, 68.68, 68.10, 65.89, 65.58, 59.42, 58.94, 57.54, 56.42, 56.06, 53.98, 53.37, 52.48, 38.70, 35.50, 31.09, 30.15, 27.29, 25.88, 20.01, 18.18, 18.00, 16.84, 16.51, 16.14, 13.17. IR (neat,  $\text{cm}^{-1}$ ): 3307 (OH), 1739, 1667 (C=O), 1158. MS ( $\text{C}_{22}\text{H}_{32}\text{N}_2\text{O}_6$ ): calcd. 421.2339 ( $[\text{M}+\text{H}]^+$ ), exp. 421.2333 ( $[\text{M}+\text{H}]^+$ ).

### 2.3. Preparation of N-Deprotected Dipeptides

To a solution of 0.25 mmol of Boc-protected dipeptides *cis*-**4** (95 mg), *trans*-**4** (95 mg), *cis*-**5** (105 mg), or *trans*-**5** (105 mg) in 1 mL dichloromethane, 0.5 mL of anisole and then 0.5 mL trifluoroacetic acid (TFA) were added. The reaction mixture was stirred at room temperature for 1 h. All volatiles were removed at reduced pressure. Dipeptides **6** and **7** were obtained quantitatively as TFA salts without further purification and were characterized by  $^1\text{H}$  NMR,  $^{13}\text{C}\{^1\text{H}\}$  NMR, and FT-IR spectroscopy as well as MS spectrometry (Figures S18–S29).

*cis*-**6**:  $^1\text{H}$  NMR (acetone- $d_6$ )  $\delta$  = 7.45–7.30 (m, 5H), 5.45 (dd,  $J$  = 25.9, 7.9, 1H), 5.21 (d,  $J$  = 4.2, 1H), 5.19–5.15 (m, 2H), 4.88–4.51 (m, 2H), 4.40–3.98 (m, 3H), 3.72–3.35 (m, 2H), 2.88–2.09 (m, 2H).  $^{13}\text{C}$  NMR ( $\text{CDCl}_3$ )  $\delta$  = 174.04, 169.26, 135.26, 128.73, 128.47, 80.89, 70.91, 67.29, 59.45, 56.97, 41.75, 36.28, 29.77, 28.43. IR (neat,  $\text{cm}^{-1}$ ): 3088 (OH and NH), 1742, 1668 (C=O), 1189, 1133 (C–O). MS ( $\text{C}_{14}\text{H}_{18}\text{N}_2\text{O}_4$ ): calcd. 279.1345 ( $[\text{M}+\text{H}]^+$ ), exp. 279.1339 ( $[\text{M}+\text{H}]^+$ ).

*trans*-**6**:  $^1\text{H}$  NMR ( $\text{CDCl}_3$ )  $\delta$  = 10.14 (bs, 1H), 8.46 (bs, 1H), 7.86 (bs, 1H), 7.38–7.22 (m, 5H), 5.53 (bs, 2H), 5.17–4.98 (m, 2H), 4.81 (bs, 1H), 4.52 (bs, 1H), 4.07 (bs, 2H), 3.63–3.11 (m, 2H), 2.52 (bs, 1H), 1.95 (bs, 1H).  $^{13}\text{C}$  NMR ( $\text{CDCl}_3$ )  $\delta$  169.66, 169.45, 135.12, 128.76, 128.70, 128.39, 127.23, 70.70, 67.56, 58.89, 54.45, 53.56, 41.66, 38.86. IR (neat,  $\text{cm}^{-1}$ ): 3088 (OH and

NH), 1745, 1667 (C=O), 1178, 1134 (C-O). MS ( $C_{14}H_{18}N_2O_4$ ): calcd. 279.1345 ( $[M+H]^+$ ), exp. 279.1339 ( $[M+H]^+$ ).

*cis*-7:  $^1H$  NMR ( $CDCl_3$ )  $\delta$  = 8.03 (d,  $J$  = 9.2, 1H), 7.41–7.27 (m, 5H), 5.25–5.04 (m, 2H), 4.52 (dd,  $J$  = 9.3, 4.8, 1H), 4.41–4.26 (m, 1H), 3.86–3.71 (m, 1H), 3.12 (dd,  $J$  = 11.1, 4.6, 1H), 2.99 (dd,  $J$  = 11.1, 1.0, 1H), 2.62–2.36 (m, 2H), 2.33–2.11 (m, 2H), 2.03 (ddd,  $J$  = 26.9, 13.4, 10.9, 1H), 0.96–0.81 (m, 6H).  $^{13}C$  NMR ( $CDCl_3$ )  $\delta$  = 175.25, 171.98, 135.54, 128.65, 128.46, 128.39, 72.07, 66.97, 59.62, 56.86, 55.25, 39.82, 31.48, 19.12, 17.64. IR (neat,  $cm^{-1}$ ): 3462, 3343, 3269 (OH and NH), 1741, 1643 (C=O), 1193, 1146 (C-O). MS ( $C_{17}H_{24}N_2O_4$ ): calcd. 321.1814 ( $[M+H]^+$ ), exp. 321.1809 ( $[M+H]^+$ ).

*trans*-7:  $^1H$  NMR ( $CDCl_3$ )  $\delta$  = 8.24 (d,  $J$  = 9.2, 1H), 7.40–7.28 (m, 5H), 5.19 (d,  $J$  = 12.2, 1H), 5.12 (d,  $J$  = 12.2, 1H), 4.49 (dd,  $J$  = 9.3, 4.9, 1H), 4.38 (bs, 1H), 4.00 (t,  $J$  = 8.4, 1H), 3.03 (d,  $J$  = 12.3, 2H), 2.75 (m, 4H), 2.28 (dd,  $J$  = 13.8, 8.7, 1H), 2.22–2.11 (m, 1H), 1.92–1.80 (m, 1H), 0.86 (dd,  $J$  = 21.9, 6.9, 6H).  $^{13}C$  NMR ( $CDCl_3$ )  $\delta$  = 175.28, 171.86, 135.53, 128.67, 128.49, 128.42, 73.10, 67.03, 59.84, 56.64, 55.52, 40.32, 31.33, 19.23, 17.64. IR (neat,  $cm^{-1}$ ): 3321 (OH and NH), 1737, 1652 (C=O), 1192, 1147 (C-O). MS ( $C_{17}H_{24}N_2O_4$ ): calcd. 321.1814 ( $[M+H]^+$ ), exp. 321.1809 ( $[M+H]^+$ ).

#### 2.4. Aldol Reactions

To **8** (151 mg, 1.0 mmol) dissolved in 2 mL of an acetone/DMSO mixture (ratio 1:5,  $v/v$ ) or in pure acetone, 20 mol-% of the solid catalyst **2**, **6**, or **7** was added after stirring overnight at room temperature. In the case of **6** and **7**, TEA was added in equimolar amounts to release the free base from the TFA salt. The reaction mixture was diluted with ethyl acetate (5 mL) and washed twice with water (2 mL). The organic layer was dried over anhydrous  $Na_2SO_4$ . The conversion number was determined by  $^1H$  NMR spectroscopy. The ee with respect to (*R*)-**9** was determined by chiral HPLC (see General Experimental Conditions). The absolute configuration of the major product was determined as *R* in accordance with the elution order in previously published data on chiral separations of **9**.

Aldol product **9**:  $^1H$  NMR ( $CDCl_3$ ):  $\delta$  = 8.21 (d,  $J$  = 8.8 Hz, 2H, H-arom), 7.54 (d,  $J$  = 8.6 Hz, 2H, H-arom), 5.26 (dt,  $J$  = 3.7 Hz, 7.6 Hz, 1H, CH-O), 3.58 (d,  $J$  = 3.3 Hz, 1H, CO-CHH), 2.85 (dd,  $J$  = 3.4 Hz, 6.1 Hz, 1H, CO-CHH), 2.22 (s, 3H, CO-CH<sub>3</sub>), 1.59 (bs, 1H, OH).  $^{13}C$  NMR ( $CDCl_3$ ):  $\delta$  = 208.47 (C=O), 149.94 (C-arom), 147.26 (C-arom), 126.37 (2  $\times$  C-arom), 123.72 (2  $\times$  C-arom), 68.86 (C-O), 51.46 (CO-CH<sub>2</sub>), 30.68 (CO-CH<sub>3</sub>).

HPLC retention time ( $t_R$ ): (*R*)-**9**: 12.2 min; (*S*)-**9**: 15.4 min (Figures S30–S39).

#### 2.5. Quantum Chemical Calculations

Conformers of free catalysts and the intermediates of the aldol reaction cycle with *cis*-**2**, *trans*-**2**, *cis*-**6**, and *trans*-**6** were modeled using the conformer search algorithm in SPARTAN (Wavefunction, Inc., Irvine, CA, USA). Geometries of transition states formed from *cis*-**2** and *trans*-**2** were modeled based on transition state geometries previously published for **1** [34,35]. All geometries were optimized at the B3LYP/6-31G(d) level with a polarized continuum model (PCM) for DMSO in GAUSSIAN 16 [36], whereby the level of theory was chosen as a compromise between accuracy and computational cost for the number of conformers that had to be optimized for this study. Geometries of transition states formed from *cis*-**6** and *trans*-**6** were modeled using the transition states from *cis*-**2** and *trans*-**2** as templates replacing the carboxylic acid –OH by Gly-OBn. Conformers were generated using a constrained conformer search with a frozen core structure, in which dihedrals were only freely rotatable for the 4-hydroxy group (provided it was not involved in the transition state) and the Gly-OBn group. Geometry optimizations at the density functional theory level were performed in a two-step procedure, first constrained (with frozen core structure) and thereafter unconstrained. Transition geometries without any precedence for L-proline such as the stereoselective step (TS4) and the alternative path for enamine formation presented in this study were modeled using the STQN method for locating transition structures [37]. TS4 geometries were modeled as transition states leading to an *R*-configured product (TS4<sub>pro R</sub>) and to an *S*-configured product (TS4<sub>pro S</sub>),



respectively, where for TS4<sub>pro R</sub> and TS4<sub>pro S</sub> each two core structures were modeled: one with an *s-anti* orientation of the enamine, and one with an *s-syn* orientation. Additional conformers with respect to 4-OH and Gly-OBn were modeled as given above. Duplicate intermediate and transition structures were identified based on their individual interatomic distance distribution pattern as described elsewhere [38], and removed using a script in MATLAB (MathWorks, Inc., Natick, MA, USA). From the transition structures, only those were kept that exhibited one imaginary frequency after frequency calculations (same level as optimizations). From the transition states with a single imaginary frequency, only those were kept, where the frequency was clearly associated with a vibration along a bond to be formed or broken in the course of the transition. For the calculation of standard free energies (*G*) from statistical thermodynamics in GAUSSIAN, all frequencies were uniformly scaled by 0.97. Average values for *G* according to the Boltzmann weights of each contributing conformer and energy barriers were calculated in MATLAB.

Theoretical enantiomeric ratios (er) *R*:*S* were calculated from the ratios of the theoretical rate constants *k<sub>R</sub>* and *k<sub>S</sub>* for the *R*- or an *S*-selective reaction steps in each modeled reaction cycle [39]. These ratios were obtained from the difference of the energy barriers Δ*G*<sub>pro R</sub> or Δ*G*<sub>pro S</sub>, i.e., the difference between free energies (Boltzmann-weighted average over different conformers) calculated for TS4<sub>pro R</sub> or TS4<sub>pro S</sub>, respectively, and the free energy of the enamine intermediate:

$$\text{er} = \frac{k_R}{k_S} = e^{-\frac{\Delta G_{\text{pro R}} - \Delta G_{\text{pro S}}}{RT}}$$

For all theoretical er values, we assumed a reaction temperature of 298.15 K.

### 3. Results

As a model reaction for asymmetric aldol additions, we used the addition of acetone to **8** to give the chiral β-hydroxyketone **9** where acetone acted both as a solvent and as a reactant. The use of a solvent mixture with DMSO (ratio DMSO/acetone 5:1, *v/v*) ensured that all reactants and catalyst were fully dissolved, as it has been shown that the catalytic cycle only involves soluble proline complexes or soluble proline adducts [40]. All reactions were carried out in the presence of 20 mol-% of the catalyst as evidenced from earlier studies as the optimal catalyst concentration [33]. After 24 h of stirring at room temperature, the overall conversion was determined by <sup>1</sup>H NMR spectroscopy and the ee by chiral phase HPLC (see Experimental Section and Figures S30–S39). **1**, *trans*-4-Hyp (*trans*-**2**), and *cis*-4-Hyp (*cis*-**2**) were used as references to evaluate the efficiency of **6** and **7** as catalysts. The results are summarized in Table 1.

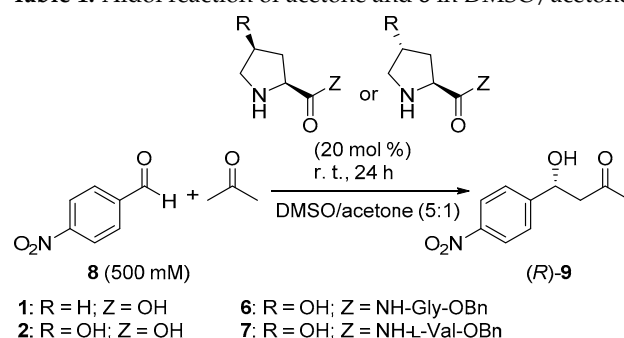
Like well-known aldol additions in the presence of **1**, catalysis with *cis*-**2** and *trans*-**2** results in virtually full conversion (>98%) after 24 h with moderate enantioselectivities in favor of the *R*-configured product (48% ee with *cis*-**2** and 40% with *trans*-**2**).

The highly similar stereochemical outcome of both conversions suggests only a little influence from the 4-hydroxy group on enantioselectivity confirming previous observations [33]. Theoretical models from previous studies on proline catalysis have shown that the stereoselectivity is determined by the relative arrangement of the double-bonded methylene group of the enamine intermediate (Scheme 1) and the carbonyl group of the substrate. Here, a coordination of the carbonyl oxygen by the carboxylic acid group of the enamine intermediate in TS4 clearly favors an *R*-configured product (TS4<sub>pro R</sub>) as the energy barrier via TS4<sub>pro R</sub> is lower than via a transition state TS4<sub>pro S</sub> with opposite arrangement.

To evaluate the plausibility of a similar mechanism with *cis*-**2** and *trans*-**2**, in analogy to previously published models for catalysis with **1**, we modeled different conformers of the enamine intermediates and of transition states TS4<sub>pro R</sub> and TS4<sub>pro S</sub> toward product **9** with both *cis*-**2** and *trans*-**2** (lowest-energy conformers of TS4<sub>pro R</sub> are depicted in Figure 2). We calculated their respective standard free energies (*G*°) at the B3LYP/6-31G(d)-level with an implicit solvent model for DMSO and determined theoretical stereoselectivities for both catalysts from the Δ*G*° values calculated with both catalysts (Table 1). The full

consideration of conformational space would require modeling numerous reaction channels for individual substrate, transition state, and product conformers and the calculation of rotational barriers to model the interconversion between different conformational species. Hence, even for systems with limited conformational space, any attempt of calculating a full reaction profile would be hardly manageable. Therefore, instead of considering free energy levels of individual conformers, we calculated free energy profiles based on Boltzmann-weighted average values of  $G^\circ$ . This approach may be a source of error, if a reaction step going through a short-lived intermediate conformer would proceed considerably faster to the next intermediate than its accommodation in a lower-lying intermediate conformer, i.e., the energy barrier by the subsequent transition state is lower than the involved rotational barriers. In all other cases, focusing on the low-lying species within a limited set of conformers appears as a good approximation, at least to obtain a qualitative picture of the energy barriers in the catalytic cycle.

**Table 1.** Aldol reaction of acetone and **8** in DMSO/acetone solvent mixture of ratio 5:1 (*v/v*).



		Conversion (%) <sup>a</sup>	ee (%) <sup>b</sup>	er (exp.) <sup>b</sup>	er (calc.) <sup>c</sup>
1	<b>1</b>	>98	64	82:18	n. d.
2	<i>cis</i> - <b>2</b>	>98	48	74:26	91:9
3	<i>trans</i> - <b>2</b>	>98	40	70:30	93:7
4	<i>cis</i> - <b>6</b>	<5	98	99:1	>99:1
5	<i>trans</i> - <b>6</b>	40	98	99:1	>99:1
6	<i>cis</i> - <b>7</b>	36	94	97:3	n. d.
7	<i>trans</i> - <b>7</b>	42	98	99:1	n. d.

In the case of **6** and **7**, triethylamine (TEA) was added in equimolar amounts to release the non-protonated catalysts from the TFA salt. <sup>a</sup> Determined by <sup>1</sup>H NMR. <sup>b</sup> Determined by chiral HPLC. <sup>c</sup> Calculated from forward rates of the stereoselective step obtained from DFT calculations.

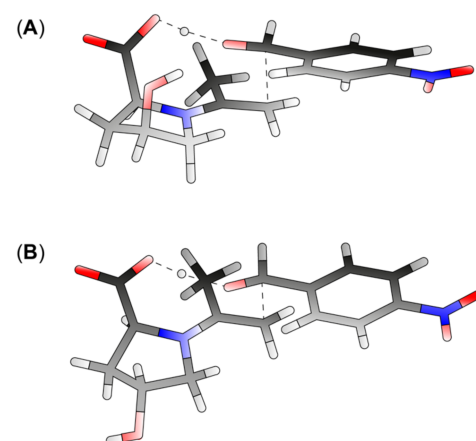


**Figure 2.** Transition states of the stereoselective step in the synthesis of **9** leading to an (*R*)-configured product (TS<sub>4<sub>pro R</sub></sub>) formed from *cis*-**2** (A) and *trans*-**2** (B).



As a first benchmark for the catalytic cycles with *cis*-2 and *trans*-2, we calculated  $\Delta G^\circ$  between enamine intermediate/substrate and TS4<sub>pro R</sub> or TS4<sub>pro S</sub>, respectively. The predicted *er* values according to the calculated  $\Delta G^\circ$  values are somewhat higher (91:9 with *cis*-2 and 93:7 with *trans*-2) than what had been observed experimentally. Still, given the low level of theory used for our calculation and the above-mentioned focus on low-lying conformers, this is in the range of the stereochemical outcome expected for proline-catalyzed aldol reactions. Taken together, transition state geometries analogous to what had been suggested previously for aldol reactions catalyzed by **1** seem to apply as well for aldol additions catalyzed by *cis*- or *trans*-2. Depending on reaction conditions, however, the *ee* of such reactions may be moderate, as the difference between energy barriers going through TS4<sub>pro R</sub> and TS4<sub>pro S</sub> is small. Interestingly, but in accordance with the experiment, the 4-hydroxy-group has little impact on the transition states shown in Figure 2, yet may have implications on ring puckering, which leads to different geometries of the lowest-energy conformers of TS4<sub>pro R</sub> with *cis*-2 (Figure 2A) and *trans*-2 (Figure 2B).

With both *cis*-2 and *trans*-2, we observed virtually full conversion (>98%) after 24 h. While C,C-bond formation is rate-limiting [12], the rate of this second-order step also depends on the concentration of the enamine intermediate, whose formation itself had previously been discussed as rate-limiting for proline-catalyzed aldol reactions [41]. To obtain a full picture of formation of enamine in the aldol reaction catalyzed by *cis*-2 in comparison to *trans*-2, we also modeled geometries of the preceding intermediates and transition states (TS1, TS2, and TS3), from formation of the hemiaminal from catalyst and acetone through the iminium intermediate to the enamine (Figure 3). To provide a rough estimate of the error due to our treatment of the conformer problem, we also plotted respective  $\Delta G^\circ$  with highest- and lowest-energy conformers as ‘whiskers’ attached to each substrate, intermediate, transition, or product state. As given in Scheme 1, we also included a parasitic side path to a putatively formed bicyclic byproduct from the iminium intermediate via TS3a in our models of reaction cycles with *cis*-2 and *trans*-2. The calculated energy barriers are reasonable in the boundaries of the accuracy of the model and are like what had been obtained for proline-catalyzed reactions previously. Differences in the energy profile of the *cis*-2 and *trans*-2 reaction cycle are small, except for the energy of the iminium intermediate being slightly lower in the *cis*-2 cycle. However, as the energy associated with hemiaminal formation, whose rate is additionally limited by concentration of reactants and the corresponding frequency factor (not considered in Figure 3), is the highest, minor differences in subsequent reaction steps should not be rate-determining. Therefore, it is not surprising that we observe very similar conversion with both catalysts after 24 h.

Reactions with catalysts *cis*-6 and *trans*-6 show with 5 and 40% low conversion after 24 h yet are highly enantioselective (98% *ee*). Reactions catalyzed by *cis*-7 and *trans*-7 confirm the moderate conversion (36% and 42%) and high enantioselectivities (94% and 98% *ee*, respectively).

In analogy to *cis*-2 and *trans*-2, we also modeled conformers of the enamine intermediates and the transition states TS4<sub>pro R</sub> and TS4<sub>pro S</sub> with *cis*-6 and *trans*-6. Due to the flexible benzylglycinate moiety, in comparison to catalysis with **1** or **2**, conformational space is considerably larger. To take this into account, we modeled 47 conformers of the *cis*-enamine and 99 of the *trans*-species and altogether 12 transition structures for the *cis* species (4 for TS4<sub>pro R</sub> and 8 for TS4<sub>pro S</sub>) and 24 for the *trans*-species (9 for TS4<sub>pro R</sub> and 15 for TS4<sub>pro S</sub>). Different from **1** and **2** catalysis, with **6**, conformers may exist that are energetically favorable, but incompatible with the transition state, for example, due to steric interference of the flexible benzylglycinate terminus with the catalytic site. Nevertheless, the theoretical rates for formation of (*R*)-**9** vs. (*S*)-**9** calculated based on Boltzmann-averaged  $\Delta G^\circ$  show a clear preference for the *R*-product (*er* > 99:1), which agrees with the high enantioselectivity observed experimentally. While the energy barriers associated with TS4<sub>pro R</sub> and TS4<sub>pro S</sub> highly vary according to the respective transition geometry conformers, the aldol reaction seems to occur predominantly via low-lying conformers of TS4<sub>pro R</sub>.

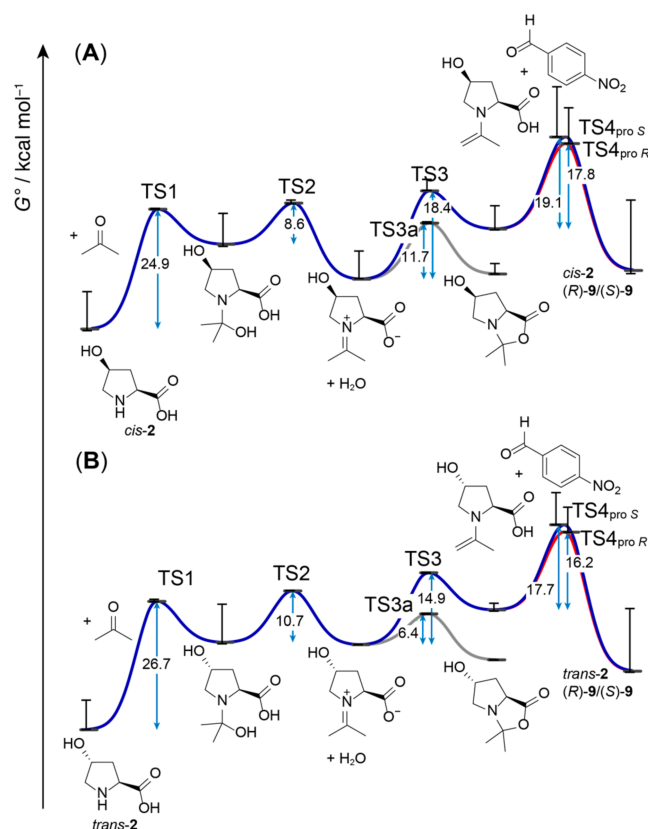


**Figure 3.** Standard transition free energies ( $\Delta G^\circ$ , represented by blue arrows) of the aldol reaction cycle catalyzed by *cis*-4-Hyp (*cis*-2) (A) and *trans*-4-Hyp (*trans*-2) (B) calculated at the B3LYP/6-31G(d) level with a solvent model for DMSO. The  $G^\circ$  levels indicated by black horizontal bars are Boltzmann-averaged over the number of conformers given in Tables S1 and S2. The whiskers (vertical lines with bars) indicate  $G^\circ$  values obtained with the lowest- and highest-energy conformers of each intermediate or transition state.

Since the proline catalysis-derived transition states of the stereoselective step of *cis*-6 and *trans*-6 catalysis successfully predict the actually observed enantioselectivities, in analogy to catalysis with **2**, we also modeled the preceding steps of aldol additions catalyzed by *cis*-6 and *trans*-6 (Figure 4). In comparison to **1** or **2**, the involved energy barriers are considerably higher, in particular, the one that corresponds to hemiaminal formation. The high barriers are due to the fact that proton transfers that are mediated by the carboxylic acid group in **1** and **2** must be undertaken by an amide in *cis*-6 and *trans*-6. Given the high  $pK$  associated with amide deprotonation (approximately 25 in DMSO) [42], intermediary formation of an amidate in analogy to a carboxylate, as with **1** or **2**, is very unlikely. Such proton transfers would be involved in TS1, formation of the hemiaminal (Figure 5A), and in TS2, elimination of water from the hemiaminal to form an iminium zwitterion. Our attempts to model TS1 involving proton transfer from the amide failed (Figure S1); however, we were able to obtain an alternative transition geometry as previously suggested by Rankin et al. for proline [35], where the hydroxylate formed upon nucleophilic attack of the nitrogen to the carbonyl takes up the proton directly from the amine instead of the amide (Figure 5B). Still, given the high energy barrier of more than 50 kcal mol<sup>-1</sup> that must be overcome for the formation of a hemiaminal from the peptide and acetone (Figure 4), a catalytic cycle as in Scheme 1 appears highly unlikely, as such a reaction would not take place at room temperature. Therefore, the whole catalytic cycle, starting with hemiaminal formation to formation of the crucial enamine intermediate, must be different in aldol additions catalyzed by peptides, in particular, those that do not feature a residue that could act as a proton donor.

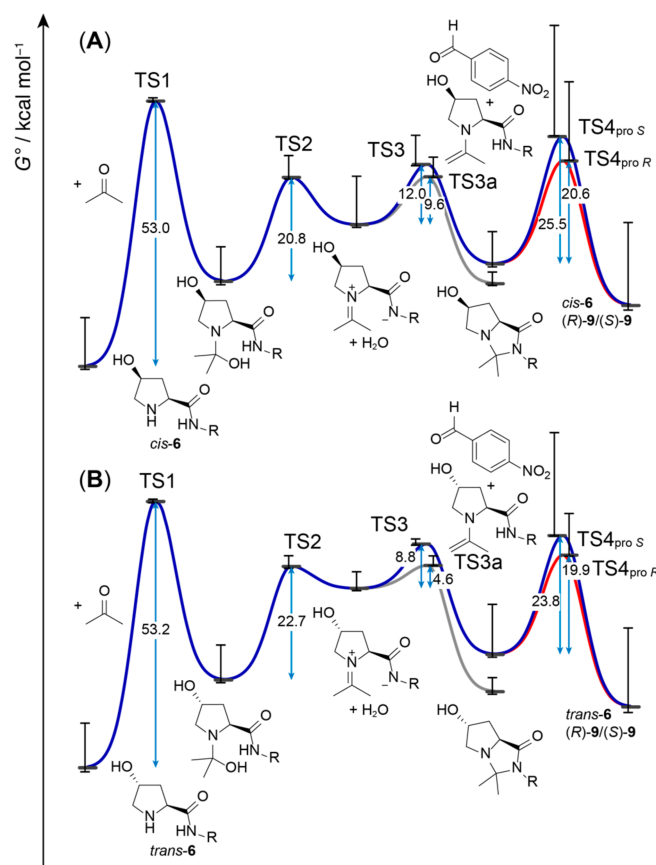


**Figure 4.**  $\Delta G^\circ$  profile of the aldol reaction cycle catalyzed by *cis*-6 (A) and *trans*-6 (B) calculated at the B3LYP/6-31G(d)/PCM (DMSO) level. The  $\Delta G^\circ$  values (blue arrows) are the differences between  $G^\circ$  levels, Boltzmann-averaged over the number of conformers given in Tables S3 and S4 (black horizontal bars). The whiskers indicate  $G^\circ$  values obtained with the lowest- and highest-energy conformers of each intermediate or transition state.

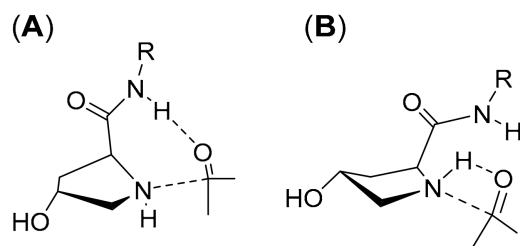
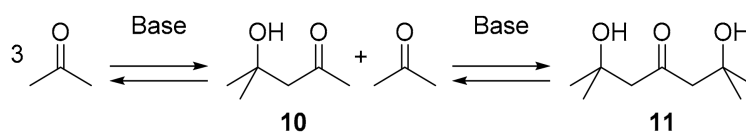


**Figure 5.** Models for transition structures towards hemiaminal formation (TS1) with a 4-Hyp peptide catalyst (here: peptide of *trans*-2). (A): hemiaminal formation involves proton transfer from the amide (in analogy to proton transfer from the carboxylic acid groups as with free amino acid catalysts). (B): direct proton transfer from the secondary amine as modeled for **1** in reference [35].

If proton transfer is not mediated by the peptide catalyst, it must occur from somewhere else. Considering the solvent DMSO as a poor proton donor, possible proton donor candidates present in the reaction solution are triethylammonium (from deprotonation of TFA salt present after Boc deprotection) or water molecules (released and taken up during reaction cycle). However, for statistical reasons, involvement of either of these very weak acids in TS1 is not very likely, as the collision frequency of three molecules in such a single third-order reaction step is expected to be very low. Furthermore, it has been shown that the presence of water has an inhibitory effect on proline-catalyzed aldol additions [43]. The last remaining candidate for a proton donor in TS1 would be the substrate, acetone, itself. A clear acetone dependence of conversion in aldol additions has been demonstrated for

formation of **9** catalyzed by L-prolineamide, a catalyst lacking a proton-donating group such as **6** and **7**: while the yield was <10% at 20 vol% acetone [44], an increase to 80% had been observed in neat acetone [45]. As a transition state where one acetone molecule protonates the other in a third-order reaction step appears highly unlikely, we abandoned the idea of considering acetone itself as a proton donor. Nevertheless, an acetone content-dependent conversion would still be observed, if, instead of acetone itself, some kind of ‘auxiliary substrate’ with proton donor properties was fed into the catalytic cycle, whose concentration depends on acetone content. A promising candidate for such an auxiliary is the acetone self-adduct **10**, which is formed from two acetone molecules halfway to trimeric acetone **11** (Scheme 3). In the presence of a base (here **6**), **10** should be present to a certain extent (equilibrium constant of  $K = 0.04$ ) [46,47].



**Scheme 3.** Aldol self-reaction of acetone.

Assuming that with a peptide catalyst, a hemiaminal is not formed from catalyst and acetone, but from acetone and **10**, proton transfer would be conveniently mediated by the  $\beta$ -hydroxy group of **10**. Due to reduced symmetry of **10** in comparison to acetone, such a transition state could be modeled with four different configurations, of which two transition state configurations lead to an *R*-configured hemiaminal, and two to an *S*-configured hemiaminal (Figure 6). Each of the four configurations allow a comparably ‘relaxed’ transition geometry comprising a six-membered ring formed from the atoms that are involved in C,C-bond formation and proton transfer.

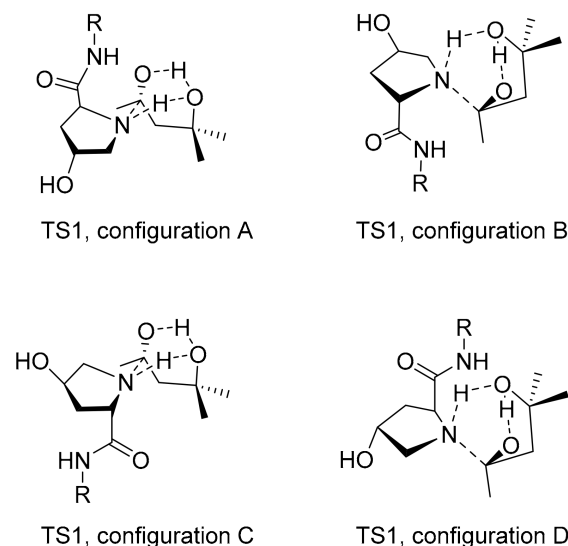
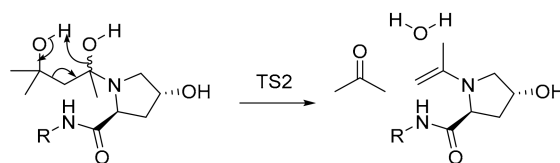


**Figure 6.** Four possible configurations (A, B, C, D) of TS1 (structure of transition state towards formation of a hemiaminal) formed from 4-Hyp-peptide catalyst (here shown for the *trans*-species) and **10**. Bonds that are formed or broken form a cyclic transition involving six atoms (dashed lines).

Similarly, starting from either an *R*- or an *S*-configured hemiaminal intermediate, formation of the enamine could as well occur via a cyclic transition state (Scheme 4). This way, the enamine is formed without the necessity of proton transfer via amide deprotonation, which would also make the formation of a parasitic bicyclic by-product less likely.



**Scheme 4.** Formation of enamine intermediate.

We calculated the transition states and intermediates from Figure 6 and Scheme 4 with 4-hydroxy-*N*-methyl-L-prolinamide (**12**) as a model peptide (Figure 7). Indeed, with 33.2 kcal/mol for TS1 (configuration A) with *cis*- and 36.6 kcal/mol for TS1 (configuration A) with *trans*-**12**, the energy barriers associated with hemiaminal formation are much lower than those found with transition geometries as in Figure 5B. Therefore, the mechanism involving **10** as a mediator does present a plausible alternative, albeit coming at the cost of a low proportion of active intermediates, as only small amounts of **10** are available. This is reflected by the considerably lower conversion observed with peptides instead of free amino acids (Table 1). With the concentration of **10** being a crucial determinant of rate and conversion, any parameter with an influence on the proportion of **10** may have an impact on conversion, such as temperature, catalyst solubility, acid/base conditions in the reaction vessel (avoiding the term ‘pH’ in the context of a DMSO solution), and the amount of excessive acetone. As particularly the latter can be easily modified, we also performed conversions in the presence of **6** and **7** in pure acetone (Table 2). As expected, the overall conversion slightly increases. Furthermore, differences in conversion between *cis*- and *trans*-configured catalysts vanish, which suggests that the very first step, the one that depends on acetone concentration, is rate-determining.

**Table 2.** Aldol reaction of acetone and **8** in pure acetone.

		Conversion (%) <sup>a</sup>	ee (%) <sup>b</sup>	er <sup>b</sup>
1	<i>cis</i> - <b>6</b>	45	98	99:1
2	<i>trans</i> - <b>6</b>	44	98	99:1
3	<i>cis</i> - <b>7</b>	85	6	47:53
4	<i>trans</i> - <b>7</b>	73	6	47:53

<sup>a</sup> Determined by <sup>1</sup>H NMR. <sup>b</sup> Determined by chiral HPLC.

For the aldol additions catalyzed by *cis*-**6** and *trans*-**6**, the high stereoselectivity reported above is fully retained in pure acetone. In contrast, it is virtually lost with both diastereomers of **7**, the catalyst with a sterically demanding L-Val sidechain. Furthermore, despite high substrate conversion, considerable formation of by-products was observed both in the presence of *cis*-**7** and *trans*-**7** (Figures S38 and S39). Possibly, in pure acetone, where higher amounts of **10** or even trimer **11** are present, alternative pathways may exist involving acetone self-adduct intermediates even at the stereoselective C,C-coupling step. If this was the case, different behavior between peptide catalysts with a more- and less sterically demanding environment around the catalytic site would be plausible.

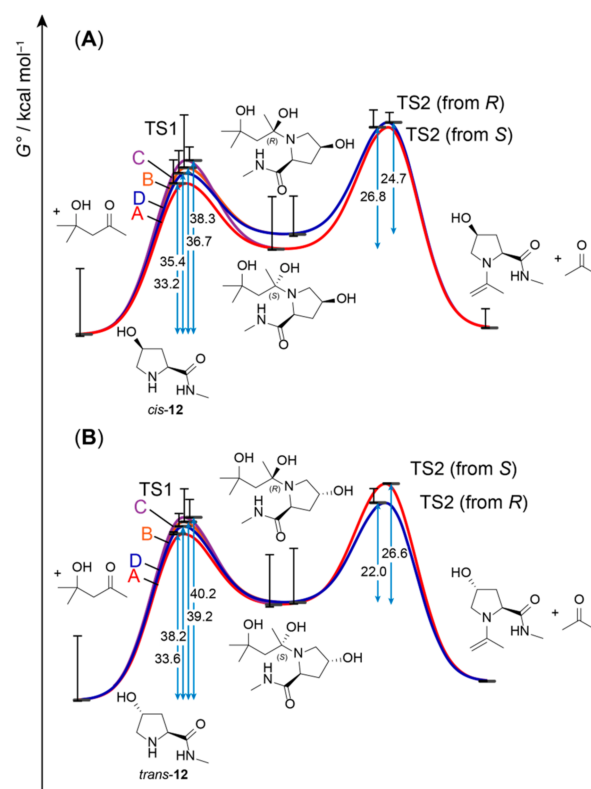


**Figure 7.** Energy barriers ( $\Delta G^\circ$ , blue arrows) in modeled catalytic pathways towards the enamine intermediates with *cis*-12 (A) and *trans*-12 (B) calculated at the B3LYP/6-31G(d)/PCM (DMSO) level. The different colors indicate different reaction channels through the four different configurations from Figure 6, two of which are going through a hemiaminal intermediate with *R*- and two with an *S*-configured hydroxy group. The whiskers represent  $G^\circ$  values obtained with the lowest- and highest-energy conformers of each intermediate or transition state. In comparison to Figure 4, the energy barrier associated with formation of a hemiaminal from peptide catalyst and 10 is much lower than for the formation of a hemiaminal from acetone.

#### 4. Discussion

Proline and hydroxyprolines catalyze stereoselective aldol additions through a highly stereospecific transition geometry consisting of a catalyst-enamine intermediate and the substrate. The enamine intermediate is formed via several reaction steps involving proton transfer to and from the carboxylic acid group of the catalyzing amino acid. An analogous catalytic cycle with peptide catalysts such as 6 and 7, which lack a proton donor, is not very plausible, as the energy barrier for formation of a hemiaminal intermediate from peptide catalyst and the electrophilic aldol component (here: acetone) is too high to be overcome at room temperature. Still, aldol additions occur with excellent stereoselectivities, albeit lower conversion in model reactions after 24 h. Our DFT calculations suggest a modified pathway that is entered by an acetone self-adduct instead of acetone in peptide-catalyzed reactions. Here, the hydroxy group of the self-adduct acts as a ‘proton-wire’, thereby easing the transfer of the proton from the catalyst nitrogen to the substrate oxygen atom. Increasing the proportion of acetone provides more acetone self-adduct, thereby increasing conversion. However, this may come at the cost of decreased stereoselectivity, which suggests that the true catalytic cycle is even more complex than the one depicted by our calculations, which demands deeper computational and experimental kinetic analyses in the future. Still, the consideration of self-adduct intermediates provides a hitherto-neglected aspect in peptide-catalyzed aldol additions and might help in the design of synthetic pathways.



**Supplementary Materials:** The following supporting information can be downloaded at: <https://www.mdpi.com/article/10.3390/chemistry5020081/s1>: Supplementary computational data (Figure S1), analytical data (Figures S2–S29), chiral phase HPLC data (Figures S30–S39), and model geometries from DFT calculations (Tables S1–S6).

**Author Contributions:** Conceptualization, L.A.M. and S.L.; methodology, L.A.M. and S.L.; software, S.L.; formal analysis, L.A.M. and S.L.; investigation, L.A.M. and S.L.; resources, H.L.; writing—original draft preparation, S.L.; writing—review and editing, L.A.M., H.L. and S.L.; visualization, S.L. All authors have read and agreed to the published version of the manuscript.

**Funding:** Experiments were carried out during a research visit financially supported by the Deutsche Forschungsgemeinschaft (DFG) and the Deutsche Akademische Austauschdienst (DAAD). For computations, the authors acknowledge support by the state of Baden-Württemberg through bwHPC and the DFG through grant no INST 40/575-1 FUGG (JUSTUS 2 cluster).

**Data Availability Statement:** Data is contained within the article or Supplementary Materials.

**Acknowledgments:** L.A.M. would like to thank Tafil Technical University (TTU) for the traveling support. Many thanks go to the NMR and MS unit at TU Chemnitz, to Nadine Killius and Michael Müller at the University of Freiburg for help with chiral HPLC, and to Wolfgang Hüttel for carefully reading the manuscript.

**Conflicts of Interest:** The authors declare no conflict of interest.

## References

1. Eder, U.; Sauer, G.; Wiechert, R. New Type of Asymmetric Cyclization to Optically Active Steroid CD Partial Structures. *Angew. Chem. Int. Ed.* **1971**, *10*, 496–497. [\[CrossRef\]](#)
2. Hajos, Z.G.; Parrish, D.R. Asymmetric Synthesis of Bicyclic Intermediates of Natural Product Chemistry. *J. Org. Chem.* **1974**, *39*, 1615–1621. [\[CrossRef\]](#)
3. Ahrendt, K.A.; Borths, C.J.; MacMillan, D.W.C. New Strategies for Organic Catalysis: The First Highly Enantioselective Organocatalytic Diels–Alder Reaction. *J. Am. Chem. Soc.* **2000**, *122*, 4243–4244. [\[CrossRef\]](#)
4. List, B. Proline-catalyzed asymmetric reactions. *Tetrahedron* **2002**, *58*, 5573–5590. [\[CrossRef\]](#)
5. Cordóva, A.; Notz, W.; Zhong, G.F.; Betancort, J.M.; Barbas, C.F., III. A Highly Enantioselective Amino Acid-Catalyzed Route to Functionalized  $\alpha$ -Amino Acids. *J. Am. Chem. Soc.* **2002**, *124*, 1842–1843. [\[CrossRef\]](#)
6. Notz, W.; Tanaka, F.; Barbas, C.F., III. Enamine-Based Organocatalysis with Proline and Diamines: The Development of Direct Catalytic Asymmetric Aldol, Mannich, Michael, and Diels–Alder Reactions. *Acc. Chem. Res.* **2004**, *37*, 580–591. [\[CrossRef\]](#)
7. Mangion, I.K.; Northrup, A.B.; MacMillan, D.W.C. The Importance of Iminium Geometry Control in Enamine Catalysis: Identification of a New Catalyst Architecture for Aldehyde–Aldehyde Couplings. *Angew. Chem. Int. Ed.* **2004**, *43*, 6722–6724. [\[CrossRef\]](#)
8. Northrup, A.B.; MacMillan, D.W.C. The First Direct and Enantioselective Cross-Aldol Reaction of Aldehydes. *J. Am. Chem. Soc.* **2002**, *124*, 6798–6799. [\[CrossRef\]](#)
9. Jarvo, E.R.; Miller, S.J. Amino acids and peptides as asymmetric organocatalysts. *Tetrahedron* **2002**, *58*, 2481–2495. [\[CrossRef\]](#)
10. Hoang, L.; Bahmanyar, S.; Houk, K.N.; List, B. Kinetic and Stereochemical Evidence for the Involvement of Only One Proline Molecule in the Transition States of Proline-Catalyzed Intra- and Intermolecular Aldol Reactions. *J. Am. Chem. Soc.* **2003**, *125*, 16–17. [\[CrossRef\]](#)
11. List, B.; Lerner, R.A.; Barbas, C.F., III. Proline-Catalyzed Direct Asymmetric Aldol Reactions. *J. Am. Chem. Soc.* **2000**, *122*, 2395–2396. [\[CrossRef\]](#)
12. Zotova, N.; Broadbelt, L.J.; Armstrong, A.; Blackmond, D.G. Kinetic and mechanistic studies of proline-mediated direct intermolecular aldol reactions. *Bioorganic Med. Chem. Lett.* **2009**, *19*, 3934–3937. [\[CrossRef\]](#)
13. Schmid, M.B.; Zeitler, K.; Gschwind, R.M. The Elusive Enamine Intermediate in Proline-Catalyzed Aldol Reactions: NMR Detection, Formation Pathway, and Stabilization Trends. *Angew. Chem. Int. Ed.* **2010**, *49*, 4997–5003. [\[CrossRef\]](#)
14. Seebach, D.; Beck, A.K.; Badine, D.M.; Limbach, M.; Eschenmoser, A.; Treasurywala, A.M.; Hobi, R.; Prikozovich, W.; Linder, B. Are Oxazolidinones Really Unproductive, Parasitic Species in Proline Catalysis?—Thoughts and Experiments Pointing to an Alternative View. *Helv. Chim. Acta* **2007**, *90*, 425–471. [\[CrossRef\]](#)
15. Sharma, A.K.; Sunoj, R.B. Enamine versus Oxazolidinone: What Controls Stereoselectivity in Proline-Catalyzed Asymmetric Aldol Reactions? *Angew. Chem. Int. Ed.* **2010**, *49*, 6373–6377. [\[CrossRef\]](#)
16. Martin, H.J.; List, B. Mining Sequence Space for Asymmetric Aminocatalysis: N-Terminal Prolyl-Peptides Efficiently Catalyze Enantioselective Aldol and Michael Reactions. *Synlett* **2003**, *2003*, 1901–1902. [\[CrossRef\]](#)
17. Shi, L.-X.; Sun, Q.; Ge, Z.-M.; Zhu, Y.-Q.; Cheng, T.-M.; Li, R.-T. Dipeptide-Catalyzed Direct Asymmetric Aldol Reaction. *Synlett* **2004**, *2004*, 2215–2217. [\[CrossRef\]](#)



18. Krattiger, P.; Kovasy, R.; Revell, J.D.; Ivan, S.; Wennemers, H. Increased Structural Complexity Leads to Higher Activity—Peptides as Efficient and Versatile Catalysts for Asymmetric Aldol Reactions. *Org. Lett.* **2005**, *7*, 1101–1103. [\[CrossRef\]](#)
19. Schnitzer, T.; Wennemers, H. Influence of the *Trans*/*Cis* Conformer Ratio on the Stereoselectivity of Peptidic Catalysts. *J. Am. Chem. Soc.* **2017**, *139*, 15356–15362. [\[CrossRef\]](#)
20. Schnitzer, T.; Wiesner, M.; Krattiger, P.; Revell, J.D.; Wennemers, H. Is more better? A comparison of tri- and tetrapeptidic catalysts. *Org. Biomol. Chem.* **2017**, *15*, 5877–5881. [\[CrossRef\]](#)
21. Kofoed, J.; Nielsen, J.; Raymond, J.L. Discovery of New Peptide-Based Catalysts for the Direct Asymmetric Aldol Reaction. *Bioorganic Med. Chem. Lett.* **2003**, *13*, 2445–2447. [\[CrossRef\]](#) [\[PubMed\]](#)
22. Metrano, A.J.; Chinn, A.J.; Shugrue, C.R.; Stone, E.A.; Kim, B.; Miller, S.J. Asymmetric Catalysis Mediated by Synthetic Peptides, Version 2.0: Expansion of Scope and Mechanisms. *Chem. Rev.* **2020**, *120*, 11479–11615. [\[CrossRef\]](#) [\[PubMed\]](#)
23. Tang, Z.; Yang, Z.-H.; Cun, L.-F.; Gong, L.-Z.; Mi, A.-Q.; Jiang, Y.-Z. Small Peptides Catalyze Highly Enantioselective Direct Aldol Reactions of Aldehydes with Hydroxyacetone: Unprecedented Regiocontrol in Aqueous Media. *Org. Lett.* **2004**, *6*, 2285–2287. [\[CrossRef\]](#) [\[PubMed\]](#)
24. Al-Momani, L.A.; Lataifeh, A. Novel O-ferrocenoyl hydroxyproline conjugates: Synthesis, characterization and catalytic properties. *Inorg. Chim. Acta* **2013**, *394*, 176–183. [\[CrossRef\]](#)
25. Crawford, J.M.; Sigman, M.S. Conformational Dynamics in Asymmetric Catalysis: Is Catalyst Flexibility a Design Element? *Synthesis* **2019**, *51*, 1021–1036. [\[CrossRef\]](#)
26. Rigling, C.; Kisunzu, J.K.; Duschmalé, J.; Häussinger, D.; Wiesner, M.; Ebert, M.O.; Wennemers, H. Conformational Properties of a Peptidic Catalyst: Insights from NMR Spectroscopic Studies. *J. Am. Chem. Soc.* **2018**, *140*, 10829–10838. [\[CrossRef\]](#)
27. Haasnoot, C.A.G.; De Leeuw, F.A.A.M.; De Leeuw, H.P.M.; Altona, C. Relationship Between Proton-Proton NMR Coupling Constants and Substituent Electronegativities. III. Conformational Analysis of Proline Rings in Solution Using a Generalized Karplus Equation. *Biopolymers* **1981**, *20*, 1211–1245. [\[CrossRef\]](#)
28. Kapitán, J.; Baumruk, V.; Kopecký, V.; Pohl, R.; Bouř, P. Proline Zwitterion Dynamics in Solution, Glass, and Crystalline State. *J. Am. Chem. Soc.* **2006**, *128*, 13451–13462. [\[CrossRef\]](#)
29. Lüdeke, S.; Pfeifer, M.; Fischer, P. Quantum-Cascade Laser-Based Vibrational Circular Dichroism. *J. Am. Chem. Soc.* **2011**, *133*, 5704–5707. [\[CrossRef\]](#)
30. Rüther, A.; Pfeifer, M.; Lórenz-Fonfría, V.A.; Lüdeke, S. pH Titration Monitored by Quantum Cascade Laser-Based Vibrational Circular Dichroism. *J. Phys. Chem. B* **2014**, *118*, 3941–3949. [\[CrossRef\]](#)
31. Shoulders, M.D.; Satyshur, K.A.; Forest, K.T.; Raines, R.T. Stereoelectronic and steric effects in side chains preorganize a protein main chain. *Proc. Natl. Acad. Sci. U.S.A.* **2010**, *107*, 559–564. [\[CrossRef\]](#)
32. Holmgren, S.K.; Taylor, K.M.; Bretscher, L.E.; Raines, R.T. Code for collagen's stability deciphered. *Nature* **1998**, *392*, 666–667. [\[CrossRef\]](#)
33. Al-Momani, L.A. Hydroxy-L-prolines as asymmetric catalysts for aldol, Michael addition and Mannich reactions. *ARKIVOC* **2012**, *6*, 101–111. [\[CrossRef\]](#)
34. Ashley, M.A.; Hirschi, J.S.; Izzo, J.A.; Vetticatt, M.J. Isotope Effects Reveal the Mechanism of Enamine Formation in L-Proline-Catalyzed  $\alpha$ -Amination of Aldehydes. *J. Am. Chem. Soc.* **2016**, *138*, 1756–1759. [\[CrossRef\]](#)
35. Rankin, K.N.; Gauld, J.W.; Boyd, R.J. Density Functional Study of the Proline-Catalyzed Direct Aldol Reaction. *J. Phys. Chem. A* **2002**, *106*, 5155–5159. [\[CrossRef\]](#)
36. Frisch, M.J.; Trucks, G.W.; Schlegel, H.B.; Scuseria, G.E.; Robb, M.A.; Cheeseman, J.R.; Scalmani, G.; Barone, V.; Petersson, G.A.; Nakatsuji, H.; et al. *GAUSSIAN 16*; Revision C.01; Gaussian Inc.: Wallingford, CT, USA, 2019.
37. Peng, C.Y.; Ayala, P.Y.; Schlegel, H.B.; Frisch, M.J. Using Redundant Internal Coordinates to Optimize Equilibrium Geometries and Transition States. *J. Comput. Chem.* **1996**, *17*, 49–56. [\[CrossRef\]](#)
38. Temerinac, M.; Reiser, M.; Burkhardt, H. Invariant features for searching in protein fold databases. *Int. J. Comput. Math.* **2007**, *84*, 635–651. [\[CrossRef\]](#)
39. Gawley, R.E. Do the Terms “% ee” and “% de” Make Sense as Expressions of Stereoisomer Composition or Stereoselectivity? *J. Org. Chem.* **2006**, *71*, 2411–2416. [\[CrossRef\]](#)
40. Iwamura, H.; Wells, D.H.; Mathew, S.P.; Klusmann, M.; Armstrong, A.; Blackmond, D.G. Probing the Active Catalyst in Product-Accelerated Proline-Mediated Reactions. *J. Am. Chem. Soc.* **2004**, *126*, 16312–16313. [\[CrossRef\]](#)
41. List, B. Enamine catalysis is a powerful strategy for the catalytic generation and use of carbanion equivalents. *Acc. Chem. Res.* **2004**, *37*, 548–557. [\[CrossRef\]](#)
42. Bordwell, F.G. Equilibrium Acidities in Dimethyl Sulfoxide Solution. *Acc. Chem. Res.* **1988**, *21*, 456–463. [\[CrossRef\]](#)
43. Zotova, N.; Franzke, A.; Armstrong, A.; Blackmond, D.G. Clarification of the role of water in proline-mediated aldol reactions. *J. Am. Chem. Soc.* **2007**, *129*, 15100–15101. [\[CrossRef\]](#) [\[PubMed\]](#)
44. Sakthivel, K.; Notz, W.; Bui, T.; Barbas, C.F., III. Sakthivel\_Amino Acid Catalyzed Direct Asymmetric Aldol Reactions—A Bioorganic Approach to Catalytic Asymmetric Carbon–Carbon Bond-Forming Reactions. *J. Am. Chem. Soc.* **2001**, *123*, 5260–5267. [\[CrossRef\]](#) [\[PubMed\]](#)
45. Tang, Z.; Jiang, F.; Cui, X.; Gong, L.Z.; Mi, A.Q.; Jiang, Y.Z.; Wu, Y.D. Enantioselective direct aldol reactions catalyzed by L-prolinamide derivatives. *Proc. Natl. Acad. Sci. USA* **2004**, *101*, 5755–5760. [\[CrossRef\]](#)

- 
46. Guthrie, J.P. Equilibrium constants for a series of simple aldol condensations, and linear free energy relations with other carbonyl addition reactions. *Can. J. Chem.* **1978**, *56*, 962–973. [[CrossRef](#)]
  47. Koelichen, K. Die chemische Dynamik der Acetonkondensation. *Z. Phys. Chem.* **1900**, *33U*, 129–177. [[CrossRef](#)]

**Disclaimer/Publisher's Note:** The statements, opinions and data contained in all publications are solely those of the individual author(s) and contributor(s) and not of MDPI and/or the editor(s). MDPI and/or the editor(s) disclaim responsibility for any injury to people or property resulting from any ideas, methods, instructions or products referred to in the content.